Naval Research Laboratory

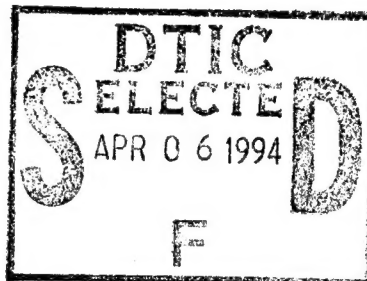Washington, DC 20375-5320

Design Considerations for a Density-Channel-Guided Laser Wake-Field Accelerator

JONATHAN KRALL

Beam Physics Branch
Plasma Physics Division

ARIE ZIGLER

Department of Physics
Hebrew University, Israel

DTIC
SELECTED
APR 0 6 1994
F

April 14, 1995

19950404 145

REPORT DOCUMENTATION PAGE

1. AGENCY USE ONLY (Leave Blank)	2. REPORT DATE	3. REPORT TYPE AND DATES COVERED
	April 14, 1995	Interim Report

4. TITLE AND SUBTITLE

Design Considerations for a Density-Channel-Guided Laser Wake-Field Accelerator

5. FUNDING NUMBERS

6. AUTHOR(S)

J. Krall and A. Zigler*

7. PERFORMING ORGANIZATION NAME(S) AND ADDRESS(ES)

Naval Research Laboratory
Washington, DC 20375-5320

8. PERFORMING ORGANIZATION REPORT NUMBER

NRL/MR/6790--95-7651

9. SPONSORING/MONITORING AGENCY NAME(S) AND ADDRESS(ES)

Office of Naval Research
Arlington, VA 22217

Department of Energy
Washington, DC 20545

10. SPONSORING/MONITORING AGENCY REPORT NUMBER

11. SUPPLEMENTARY NOTES

*Department of Physics, Hebrew University, Israel

12a. DISTRIBUTION/AVAILABILITY STATEMENT

12b. DISTRIBUTION CODE

13. ABSTRACT (Maximum 200 words)

A self-modulated laser wake-field accelerator configuration in which the laser pulse is optically guided by a plasma density channel is considered. Preliminary experiments on the generation of a plasma channel by a slow capillary discharge are described. It is shown that homogeneous channels with length $L_{chann} \gg \lambda_p$ can be produced, where λ_p is the plasma wavelength. Key issues are addressed, including phase detuning between the accelerated electron bunch and the wake field, beam-plasma and laser-plasma instabilities, and the effect of density variations that might occur over the length of the plasma channel. Numerical simulations, using present experimental parameters, show accelerating gradients in excess of 50 GV/m.

14. SUBJECT TERMS

Laser-plasma
Particle acceleration

15. NUMBER OF PAGES

22

16. PRICE CODE

17. SECURITY CLASSIFICATION OF REPORT	18. SECURITY CLASSIFICATION OF THIS PAGE	19. SECURITY CLASSIFICATION OF ABSTRACT	20. LIMITATION OF ABSTRACT
UNCLASSIFIED	UNCLASSIFIED	UNCLASSIFIED	UL

CONTENTS

Design Considerations for a Density-Channel-Guided Laser Wake-Field Accelerator

I. Introduction

Experimental studies of intense laser pulse propagation in plasmas will have an important impact on a variety intense laser applications, such as laser-driven plasma accelerators [1-7], x-ray lasers and laser fusion concepts. Through the use of optical guiding, a laser pulse can propagate over distances larger than the vacuum diffraction (Rayleigh) length. One method of optically guiding a high-intensity laser pulse is by using a preformed plasma density channel. In plasma channel guiding, one tailors transverse density of the plasma so that the minimum is at the center of the laser pulse. This guiding is linear and thus works independently of laser power, even at high power[8]. The large amplitude plasma wave (wake field) that can be excited by an intense laser pulse propagating through a plasma channel can be used to trap and accelerate electrons.

In this report, we consider the guiding of a laser pulse in plasma channel generated by a slow capillary discharge. In this process, an electrical discharge heats a capillary plasma. The plasma radiates, providing further evaporation of the capillary walls. A laser pulse propagating within the resulting plasma density channel excites a surface mode on the inside of the channel. The wake field extends into the center of the channel to produce an uniform accelerating field over distances of tens of diffraction lengths.

Plasma-based accelerators have recently been the subject of extensive research because of their potential for high accelerating gradients, compact size and low cost compared with conventional rf-driven accelerators. Plasma-based accelerator concepts rely on the transformation of energy from either a laser pulse or an electron pulse to generate a large-amplitude wake field. The laser wake-field accelerator (LWFA)[1-5] and the plasma beat wave accelerator (PBWA)[6,7] are two important laser-driven accelerator schemes.

In the LWFA, a short ($\tau_L < 1$ ps), high power ($P \sim 1$ TW) laser pulse propagates in a plasma to generate a large amplitude ($E > 1$ GV/m) wake field. The wake field is generated by the ponderomotive force exerted on the plasma electrons by the laser pulse. Because the phase velocity of the wake field is equal to the group velocity of the laser

pulse ($v_{ph} = v_{g,laser}$), a properly phased electron bunch can be simultaneously focused and accelerated. The energy of the light pulse is thus transformed into kinetic energy of the electron bunch. Laser systems based on the chirped-pulse amplification technique are capable of delivering the short (< 1 ps), ultrahigh power (~ 1 TW) laser pulses required by the LWFA[9,10].

Two configurations of the LWFA have been theoretically and numerically investigated: (i) the "standard" LWFA[1-3] and (ii) the recently proposed self-modulated laser wake-field accelerator (SM-LWFA)[4,5], in which enhanced wake field amplitudes and enhanced acceleration are obtained.

A. Standard Laser Wake-Field Acceleration

In the standard LWFA, efficient wake generation requires $L \simeq \lambda_p/2$, where L is defined to be the full-width-at-half-maximum length of the laser intensity profile on axis, $\lambda_p = 2\pi c/\omega_p$ is the plasma wavelength, $\omega_p = (4\pi n_0 e^2/m)^{1/2}$ and n_0 is the ambient plasma density. In the mildly relativistic limit ($a_0^2 \ll 1$), the peak axial electric field in the standard LWFA configuration is given by[3]

$$E_{max}[\text{GV/m}] \simeq 5.9 \times 10^4 \frac{\lambda_0^2}{r_0^2} \frac{P[\text{TW}]}{\lambda_p[\mu\text{m}]}, \tag{1}$$

where r_0 is the radius of the minimum laser spot size, λ_0 is the laser wavelength, P is the peak laser power and a linearly polarized laser has been assumed. The laser power P is related to the laser spot size r_0, wavelength λ_0, and strength parameter a_0 by

$$P[\text{GW}] \simeq 21.5(a_0 r_0/\lambda_0)^2, \tag{2}$$

assuming a Gaussian radial profile. The strength parameter a_0 is related to the peak laser pulse intensity I by

$$a_0 \simeq 8.5 \times 10^{-10} \lambda_0[\mu\text{m}]I^{1/2}[\text{W/cm}^2]. \tag{3}$$

The energy gain of an electron from the wake field is roughly the product of the accelerating field given by Eq. (1) and the effective interaction distance. Without optical guiding, the interaction distance is limited to $L_{int} = \pi Z_R$, where $Z_R = \pi r_0^2/\lambda_0$ is the Rayleigh length.

To improve the final energies of accelerated particles in the LWFA, higher accelerating fields and longer interaction distances are required. Accelerating fields can be increased by

2

reducing the laser pulse-length, which is limited by technological considerations. Longer interaction distances may be achieved if the laser pulse can be optically guided[8,11,12].

B. Self-Modulated Laser Wake-Field Acceleration

In the recently proposed self-modulated LWFA[4,5], enhanced electron acceleration is achieved via resonant self-modulation of the laser pulse[4,5,13]. This occurs when (i) the laser pulse extends axially over several plasma wavelengths, $L > \lambda_p$, and (ii) the peak laser power satisfies $P \geq P_c$, where P_c is the critical power for relativistic optical guiding[14],

$$P_c[\text{GW}] \simeq 17(\lambda_p/\lambda_0)^2. \tag{4}$$

At fixed laser parameters, both conditions can be met by choosing a sufficiently high plasma density. This is the case since $P_c \sim 1/n_0$ and $\lambda_p \sim 1/n_0^{1/2}$. Operation in the self-modulated regime has very significant advantages over the standard configuration.

Wake fields generated in the self-modulated regime are more than an order of magnitude greater than those generated by a laser pulse with $L = \lambda_p/2$, assuming fixed laser parameters. Acceleration is enhanced for four reasons. First, a higher density produces a larger wake field: $E_z \sim n_0^{1/2}$. Second, the resonant mechanism excites a very-high-amplitude wake field in comparison to the standard LWFA. Third, since $P \geq P_c$, relativistic focusing[14,4,2,11] further enhances the laser intensity, increasing a_0. Fourth, simulations show that a portion of the pulse will remain guided over multiple laser diffraction lengths, extending the acceleration distance. In the SM-LWFA, the maximum electric wake field E_{max}, is typically on the on the order of $E_{WB} = mc\omega_p/e$, where E_{WB} is the non-relativistic wave-breaking field.

The self-modulation mechanism can be understood by considering a long laser pulse having $L \gg \lambda_p$, with power $P > P_c$, such that the body of the pulse is relativistically guided[11]. The leading edge of the pulse will create a low-amplitude wake field within the remainder of the laser pulse. Alternatively, this plasma wave can be generated via a forward Raman scattering (FRS) instability[15]. In the wake field, each region of decreased density acts as a local plasma channel to enhance the relativistic focusing effect, while each region of increased density causes defocusing. This results in a low-amplitude modulation of the laser pulse at λ_p. The modulated laser pulse resonantly excites the wake field and the

3

process continues in an unstable manner. This instability, which is observed to develop on a time-scale associated with laser diffraction, resembles a highly nonlinear two-dimensional form of the usual FRS instability. It is distinguished from FRS by its two-dimensional nature and by its growth rate, which increases dramatically as the $P \geq P_c$ threshold is crossed.

C. A Proposed Channel-Guided SM-LWFA Experiment

If no optical guiding is present, the interaction length is determined by the diffraction of the laser pulse. The interaction length can be substantially increased if the focused laser pulse is optically guided by a preformed plasma channel. Demonstration of such guiding over a channel length $L_{chan} = 1$ cm in a capillary produced plasma channel is one of the major tasks of a proposed experiment to take place at Hebrew University (HU). For the experimental parameters, given in Table I, $L_{chan} = 32 Z_R$.

For these parameters, the standard LWFA requires $\lambda_p = 2L = 60$ μm ($n_0 = 3.1 \times 10^{17} \text{cm}^{-3}$), such that Eq. (1) gives $E_{max} = 1.9$ GV/m. The energy gain is then limited to $\Delta W_{max} = E_{max} L_{chan} = 19$ MeV.

By contrast, simulations of a SM-LWFA configuration, based on experimental parameters, show a significant improvement, with peak accelerating fields in excess of 50 GV/m. Thus, the HU experiment will be rely on the SM-LWFA concept. In a later stage of the experiment, an attempt will be made to couple an electron beam injector (750 kV Febetron) with the HU laser system. If successful, electrons with energies of several tens of MeV will be detected.

In this report, a SM-LWFA configuration in which the laser pulse is optically guided will be considered. In Section II, the issue of phase detuning between the accelerated electron bunch and the wake field will be discussed. In Section III, beam-plasma and laser-plasma instabilities will be considered. In Section IV, simulation results on laser guiding, laser modulation and wake field generation will be presented. Preliminary experimental results on the generation of a plasma channel by a capillary discharge will be discussed in Section V. The paper concludes with Section VI.

4

II. Phase Detuning

For a laser pulse with $P \sim 1$ TW, operation at $P \sim P_c$ implies a high plasma density $(n_p \sim 10^{19}$ cm$^{-3})$. At such high densities, the phase velocity of the wake field is reduced:

$$\gamma_{ph} = \gamma_{g,laser} \simeq \frac{\lambda_p}{\lambda_0} \gamma_{\perp}, \tag{5}$$

where $\gamma_{\perp} = (1 + a_0^2/2)^{1/2}$. Simulations[4] show that acceleration in this regime can be limited by phase detuning[16]:

$$\Delta W_{max} = \frac{2}{\pi} e E_{max} \lambda_p \gamma_{ph}^2 = \frac{2}{\pi} e E_z \frac{\lambda_p^3}{\lambda_0^2} \gamma_{\perp}^2. \tag{6}$$

Detuning of the synchronization between the wake field and the accelerated electron bunch occurs when the electron bunch "out runs" the wake field. Equation (6) illustrates the trade-off between detuning length $(L_d \sim 1/n_p^{3/2})$ and accelerating gradient $(E_{max} \sim n_p^{1/2})$ as n_p is varied. For the SM-LWFA, energy gain is optimum at the lowest density for which laser self-modulation occurs, assuming that the laser pulse can be guided over an appropriately long distance. For the parameters of Table I, $\Delta W[\text{MeV}] \simeq 1.7 E_{max}[\text{GV/m}]$ and $E_{WB} \simeq 270$ GV/m.

When used in a SM-LWFA configuration, the preformed plasma density channel increases the energy gain in two important ways: a) the pulse can be guided over very long distances (tens of Z_R) and b) the $P \geq P_c$ requirement for self-modulation is relaxed in a plasma density channel.[13]

III. Beam and Laser Instabilities

A. Beam-Plasma Two-Stream Instability

The electron two-stream instability is not an issue for the parameters of Table I. The saturation amplitude of the two-stream instability[17], due to particle trapping, is given by $E_{TS} = 8\pi\gamma n_b mc^2 S$, where $S = \beta^2\gamma(n_b/2n_0)^{1/3} \ll 1$, $\gamma = (1-\beta^2)^{-1/2}$ is the relativistic factor of the injected electron beam, n_b is the beam density, and E_{TS} is the saturation amplitude of the electric field associated with the two-stream instability. The ratio of the saturation amplitude of the two-stream field to the amplitude of the wake field is given by $E_{TS}/E_{WB} \simeq 2\beta\gamma(n_b/2n_0)^{2/3} < 10^{-4}$. For the parameters in Table I, $E_{TS}/E_{WB} < 10^{-4}$. Hence, the two-stream instability is not a problem.

B. Laser-Plasma Instabilities

Various laser-plasma instabilities could affect the propagation of the laser pulse. In particular, Raman back scatter (RBS) and Raman side scatter (RSS) are not included in the numerical simulations, could degrade the laser pulse energy[18-22]. Saturation of RBS occurs due to particle trapping[18,19]. The ratio of the back scattered power at saturation to the laser pulse power is given by $P_{RBS}/P = (\lambda_0^2/2a_0\lambda_p^2)^{4/3}$, where $a_0 < 1$ is assumed. For the simulation parameters, $P_{RBS}/P = 8.5 \times 10^{-4}$. Hence, after propagating 0.1 cm, less than 0.5 % of the laser pulse energy will be back scattered. An additional problem is RSS, which can cause the tail of the laser pulse to erode[20]. This can limit the effective length of the laser pulse. As with RBS, RSS saturates due to particle trapping[23]. The saturation power is estimated to be $P_{RSS}/P = 10^{-3}$, implying an energy loss on the order of one percent during the 0.1 cm propagation.

Some difficulty may arise due to the laser-hose (LH) instability[24,25]. In general, asymptotic growth rates for self-modulation, FRS and LH are comparable, with similar scaling with respect to laser power, pulse length, and propagation distance. Numerical modeling of the coupled LH and self-modulation instabilities[25] shows that the initial perturbation for self-modulation is the wake field, which can be quite strong. By contrast, the perturbations which can drive LH are a)"noise" in the laser centroid and b) misalignment between the direction of laser propagation and the channel axis. As a result,

self-modulation will dominate if the LH perturbations are sufficiently small (on the order of a few percent, relative to the spot size of the laser).

IV. Simulation: Laser Guiding and Modulation

We have performed simulations of laser pulse self-modulation, channel guiding, and wake field generation for laser and plasma parameters corresponding to the proposed experimental values. Several simulations were performed to optimize the final particle energy [Eq. (6)] as a function of the on-axis plasma density for fixed laser parameters.

Possible variations in the plasma density along the length of the channel were also considered. The simulation presented below shows that the laser pulse remains guided even with significant variations in the on-axis channel density, as long as the on-axis density remains sufficiently below the density at the outer edge of the channel. This is true, in general, because typical channel radii are $r_{chan} \sim 100$ μm, while the typical laser spot size is $r_0 \sim 10$ μm.

In the simulation, the initial on-axis density is $n_0 = 8.0 \times 10^{18}$ cm^{-3} ($\lambda_p = 12$ μm). The plasma density varies parabolically versus radius to a density of $3n_0$ at the channel edge ($r_{chan} = 40$ μm). Over the length of the 1 cm simulation, the on-axis density increases linearly to $2n_0$. The simulation was performed using the LEM[26] nonlinear fluid simulation model, which uses "speed of light" coordinates (r, $\zeta = z - ct$, $\tau = t$).

The 0.3 TW laser has parameters given in Table I. Figure 1 shows the modulated laser pulse after $c\tau = 0.75$ cm of propagation. In the figure, the direction of laser propagation is towards the right. A plot of the laser power vs ζ at $c\tau = 0.75$ cm, Fig. 2, shows that the laser power is also modulated. This indicates that the modulation is dominated by FRS (by contrast, self-modulation of the laser envelope[13] does not modulate the radially-integrated laser power[4,5,13]).

The plasma density wake is shown in Fig. 3, which also illustrates the density channel profile. The corresponding on-axis electric wake field, shown in Fig. 4 exceeds 50 GV/m. With $\lambda_p = 12$ μm, $\lambda_0 = 1.0$ μm, $a_0 = 0.38$ and $E_z = 50$ GV/m, Eq. (6) indicates a maximum energy gain > 55 MeV for this case.

8

V. Experiment: Plasma Density Channel Generation

Production of a plasma with dimensions $\gg \lambda_p$ by an electrical discharge through a slotted capillary insulator has been proposed previously[27-30]. An electrical discharge heats the capillary plasma that radiates and provides further evaporation of the capillary walls. The created plasma flows into a vacuum cell through a slit in the anode (the anode channel). The plasma density and profile is controlled by varying the discharge parameters. The homogeneity of the plasma jet is obtained by using a long anode channel made out of an alloy with a high thermal conductivity.

In preliminary experiments, a plasma was produced by a discharge through the capillary. The capillary consisted of a 10 mm long Teflon cylinder, with a 0.1 mm $\times$ 9 mm slit along it. This cylinder was placed between two electrodes connected to a 36 mF capacitor. The created plasma flowed out through a 0.1 mm $\times$ 10 mm anode channel. The capacitor voltage varied from 2 to 4 kV. The discharge was triggered by a third electrode by using a high voltage short pulse. At high discharge voltages the plasma density at the anode exit exceeds 2×10^{20} cm^{-3}[30]. When an anode made from a high thermal-conduction material with a high evaporation temperature (W-Cu alloy) was used, the anode wall ablation was reduced to a few percent of the total ablation.

Information on plasma jet homogeneity and jet expansion near the anode exit was derived from images collected by the frame camera. Results show that the characteristics of plasma flow through the 25 mm long anode channel vary and can be divided into two regimes. In the case of low voltage (below 2.3 kV), the plasma jet duration is about 40% longer than the ohmic heating pulse. The jet homogeneity is slightly better than in the case of the shorter anode channel, the jet velocity is slightly lower, and the expansion angle at the anode exit is about 15°. When the discharge voltage reaches a value of 2.3 kV there is a conspicuous change in the flow process. The jet duration is about 7 times longer than the ohmic heating pulse. The first 10 ms of the flow is quite similar to the case of low energies, but afterwards the spatial homogeneity of the jet is much improved and the expansion angle at the anode exit is reduced to a few degrees. The jet velocity is about 3×10^5 cm/sec.

9

A possible explanation of the increased jet duration and the improved homogeneity in the case of the long anode channel can be related to the influence of viscous forces. These frictional forces opposing the flow direction are proportional to the flow velocity. In order to enable a steady flow, the pressure gradient should balance the frictional forces. This gradient is given by $P = -12\rho\nu\langle v\rangle/d^2$, where ρ is the fluid density, ν is the kinematic viscosity coefficient, d is the distance between channel walls and $\langle v\rangle$ is the average flow velocity. Thus, using the equation of state of an ideal gas and assuming a steady flow we can estimate $T = -12m_a\nu\langle v\rangle/d^2$, where m_a is the atomic weight.

The estimated plasma temperature inside the capillary is 3.5 eV, leading to a temperature drop of about 2.5 eV (from 3.5 eV to 1 eV) along the first 10 mm of flow. This gradient accelerates the plasma jet up to above 5×10^5 cm/sec. For our experimental conditions of plasma temperature of 1eV and density of 10^{20} cm^{-3}, the viscosity coefficient of the teflon plasma is 2.35 cm^2/sec. The distance between the anode channel walls is 0.2 mm. Thus, in order to overcome the frictional forces, the required temperature gradient is 0.67 eV/cm. The required gradient is proportional to the square root of the temperature and inversely proportional to the density. Such a temperature gradient can be achieved at initial stages of the discharge when the outer region of the anode channel is cold due to the high heat conductivity of W-Cu alloy.

At a later time, when the plasma jet heats the anode walls to about 0.3 eV, the conductivity is reduced and the temperature gradient of plasma jet becomes too small to support the jet velocity. Due to the flow rate reduction, the plasma remains for a longer period in the capillary. Therefore wall ablation continues for a much longer time than the first half cycle of the electric discharge and a large amount of plasma is generated. The plasma ablated in the late stages of the discharge is much cooler than during the first half cycle. Thus the pressure gradient is reduced and the plasma inhomogeneities are smoothed. This phenomenon has a positive feedback. Reduction of flow rate causes a reduction of the temperature and the pressure gradients, which in turn reduces the jet velocity and leads to further improvement of the homogeneity.

The plasma density profile was simply controlled by a change of the applied voltage. The density profile was measured by an x-ray absorption technique using x-rays from the

10

laser produced plasma. The Abel inversion technique was applied to determine the plasma profile. The plasma density profile found to be parabolic[29].

VI. Conclusions

In this report, we have considered a self-modulated laser wake-field accelerator configuration in which the laser pulse is optically guided by a plasma density channel. The preliminary experimental results of Sec. V show that long plasma channels with $L_{chan} \gg \lambda_p$ can be generated by a slow capillary discharge.

Various key issues affecting laser propagation and electron acceleration were addressed. Specifically, beam-plasma and laser-plasma instabilities were considered. While Raman back scatter and Raman side scatter were found to have no significant impact, the laser-hose instability may be observable in the experiment if the laser focus and the plasma channel are significantly misaligned. Also, it was shown that phase slippage between the accelerated electron bunch and the wake field limits the acceleration for the high plasma density ($\sim 10^{19}$ cm^{-3}) considered here. This high density is required to obtain self-modulation, which resonantly drives the plasma wake.

Finally, numerical simulations using present experimental parameters (Sec. IV) showed that the laser pulse can be guided by such a channel and that, once laser modulation occurs, accelerating gradients in excess of 50 GV/m should be observable. The simulations also show that the laser pulse will remain guided even with significant variations in the on-axis channel density, as long as the on-axis density remains below the density at the outer edge of the channel. This result reflects the fact that the channel radius generated by the capillary-discharge is $r_{chan} \simeq 50$ μm $\gg r_0 \simeq 10$ μm, where r_0 the laser spot size at focus.

Acknowledgements

References

1. T. Tajima and J. M. Dawson, Phys. Rev. Lett. **43**, 267 (1979).

2. P. Sprangle, E. Esarey, A. Ting and G. Joyce, Appl. Phys. Lett. **53**, 2146 (1988).

3. E. Esarey, A. Ting, P. Sprangle and G. Joyce, Comments Plasma Phys. Controlled Fusion **12**, 191 (1989).

4. J. Krall, A. Ting, E. Esarey and P. Sprangle, Phys. Rev. E **48**, 2157 (1993).

5. N. E. Andreev, L. M. Gorbunov, V. I. Kirsanov, A. A. Pogosova and R. R. Ramazashvili, Pis'ma Zh. Eksp. Teor. Fiz. **55**, 551 (1992).

6. C. Joshi, W. B. Mori, T. Katsouleas, J. M. Dawson, J. M. Kindel and D. W. Forsulund, Nature **311**, 525 (1984).

7. C. E. Clayton, K. A. Marsh, A. Dyson, M. Everett, A. Lal, W. P. Leemans, R. Williams and C. Joshi, Phys. Rev. Lett. **70**, 37 (1993).

8. P. Sprangle, E. Esarey, J. Krall and G. Joyce, Phys. Rev. Lett. **69**, 2200 (1992).

9. P. Maine, D. Strickland, P. Bado, M. Pessot and G. Mourou, IEEE J. Quant. Electronics **24**, (1988).

10. G. Mourou and D. Umstadter, Phys. Fluids B **4**, 2315 (1992).

11. A. Ting, E. Esarey and P. Sprangle, Phys. Fluids B **2**, 1390 (1990).

12. C. G. Durfee III and H. M. Milchberg, Phys. Rev. Lett. **71**, 2409 (1993).

13. E. Esarey, J. Krall and P. Sprangle, Phys. Rev. Lett. **72**, 288 (1994).

14. C. E. Max, J. Arons and A. B. Langdon, Phys. Rev. Lett. **33**, 209 (1974).

15. C. Joshi, T. Tajima, J. M. Dawson, H. A. Baldis and N. A. Ebrahim, Phys. Rev. Lett. **47**, 1285 (1981).

16. E. Esarey and M. Pilloff, "Maximum Energy Gain in a Nonlinear Plasma Wave", submitted to Proceedings of the 6*th* Workshop on Advanced Accelerator Concepts, Lake Geneva, Wisconsin, 1994.

17. M. Lampe and P. Sprangle, Phys. Fluids **18**, 475 (1975).

18. P. Sprangle and E. Esarey, Phys. Rev. Lett. **67**, 2021 (1991).

19. E. Esarey and P. Sprangle, Phys. Rev. A **45**, 5872 (1992).

20. T. M. Antonsen, Jr., and P. Mora, Phys. Rev. Lett. **69**, 2204 (1992); Phys. Fluids B **5**, 1440 (1993).

21. C. B. Darrow, C. Coverdale, M. D. Perry, W. B. Mori, C. Clayton, K. Marsh and C. Joshi, Phys. Rev. Lett. **69**, 442 (1992).

22. W. P. Leemans, C. E. Clayton, W. B. Mori, K. A. Marsh, P. K. Kaw, A. Dyson, C. Joshi and J. M. Wallace, Phys. Rev. A **46**, 1091 (1992).

23. E. Esarey and P. Sprangle (private communication, 1994).

24. J. S. Wurtele and G. Shvets, Bull. Am. Phys. Soc. **38**, 1998 (1993).

25. P. Sprangle, J. Krall and E. Esarey, to appear in Phys. Rev. Lett. (1994).

26. J. Krall, E. Esarey, P. Sprangle and G. Joyce, Phys. Plasmas **1**, 1738 (1994).

27. A. Zigler, M. Kishenevsky, M. Givon and B. Arad, Phys. Rev. A **35**, 4446, 1987

28. R. W. Lee and A. Zigler, Appl. Phys. Lett. **53**, 21 (1988).

29. B. Brill, B. Arad, M. Kishenevsky and A. Zigler, J. Phys. D **23**, 1064 (1990).

30. A. Zigler, J. Erlich and C. Cohen, to appear in Appl. Phys. Lett. (1994).

Table I: Parameters of HU/NRL Experiment

Laser Parameters

Wavelength (λ)	1.0 μm
Energy	30 mJ
Pulse length (τ_L, L/c)	100 fs
Focal spot radius (r_L)	10 μm
Intensity	2×10^{17} W/cm^2
Power (P)	0.3 TW
Strength parameter (a_0)	0.38
Rayleigh length (Z_R)	0.3 mm

Wake Field Parameters

Plasma density (n_0)	8.0×10^{18} cm^{-3}
Plasma wavelength (λ_p)	12 μm
Plasma channel length (L_{chan})	1 cm
Acceleration gradient (E_z)	> 50 GV/m
Energy gain	> 55 MeV

Electron Beam Parameters (HU Febetron)

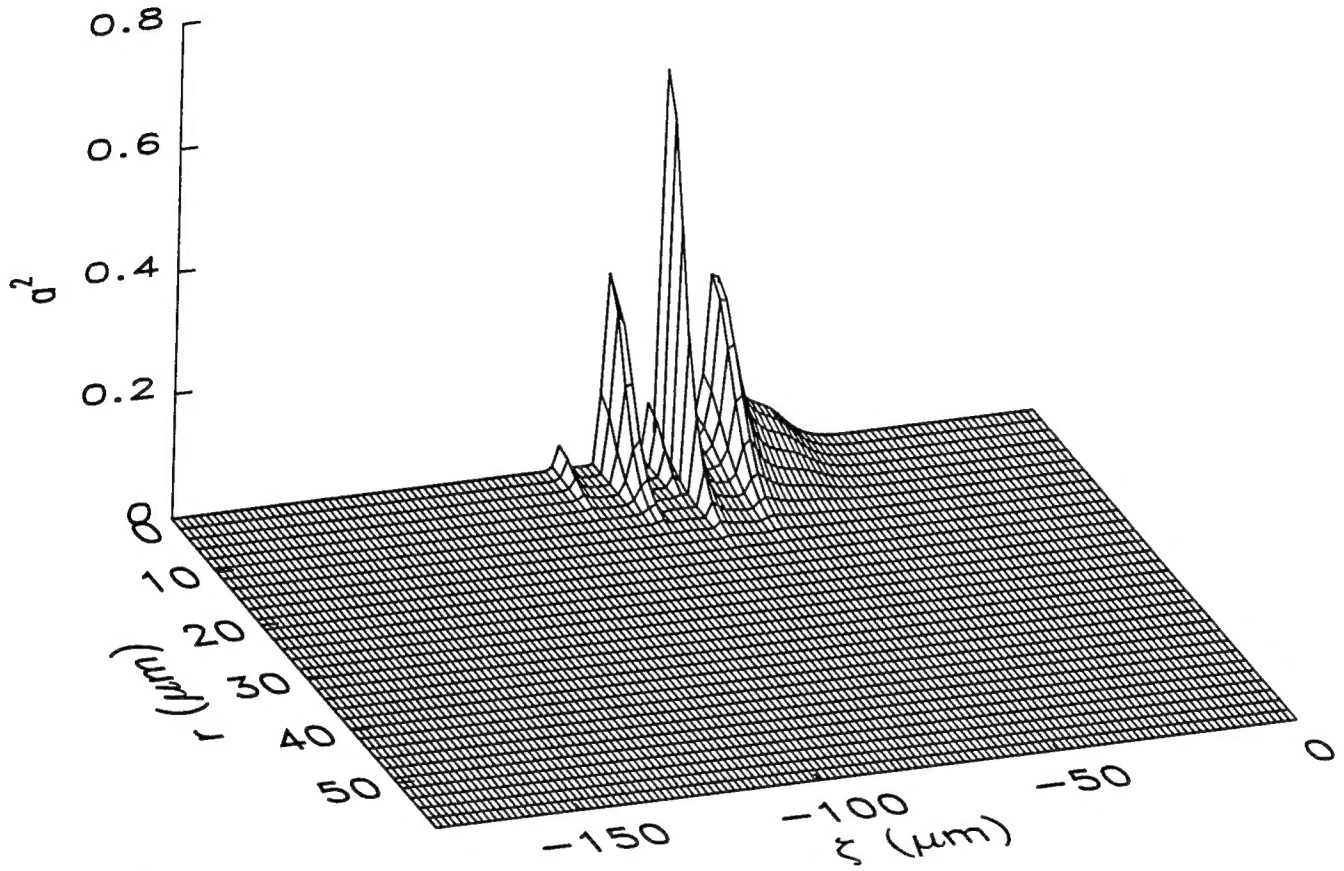|	
Bunch duration (τ_e)	50 ns
Focused beam radius (r_e)	100 μm
Injection energy	750 KeV
Current	10 A
Number of electrons trapped	10^5

Fig. 1 — Laser intensity $|\hat{a}_f|^2$, sampled over a coarse grid (the numerical grid is much finer), at $c\tau = 0.75$ cm ($24Z_R$) shows modulation of the laser pulse. The direction of propagation is towards the right.
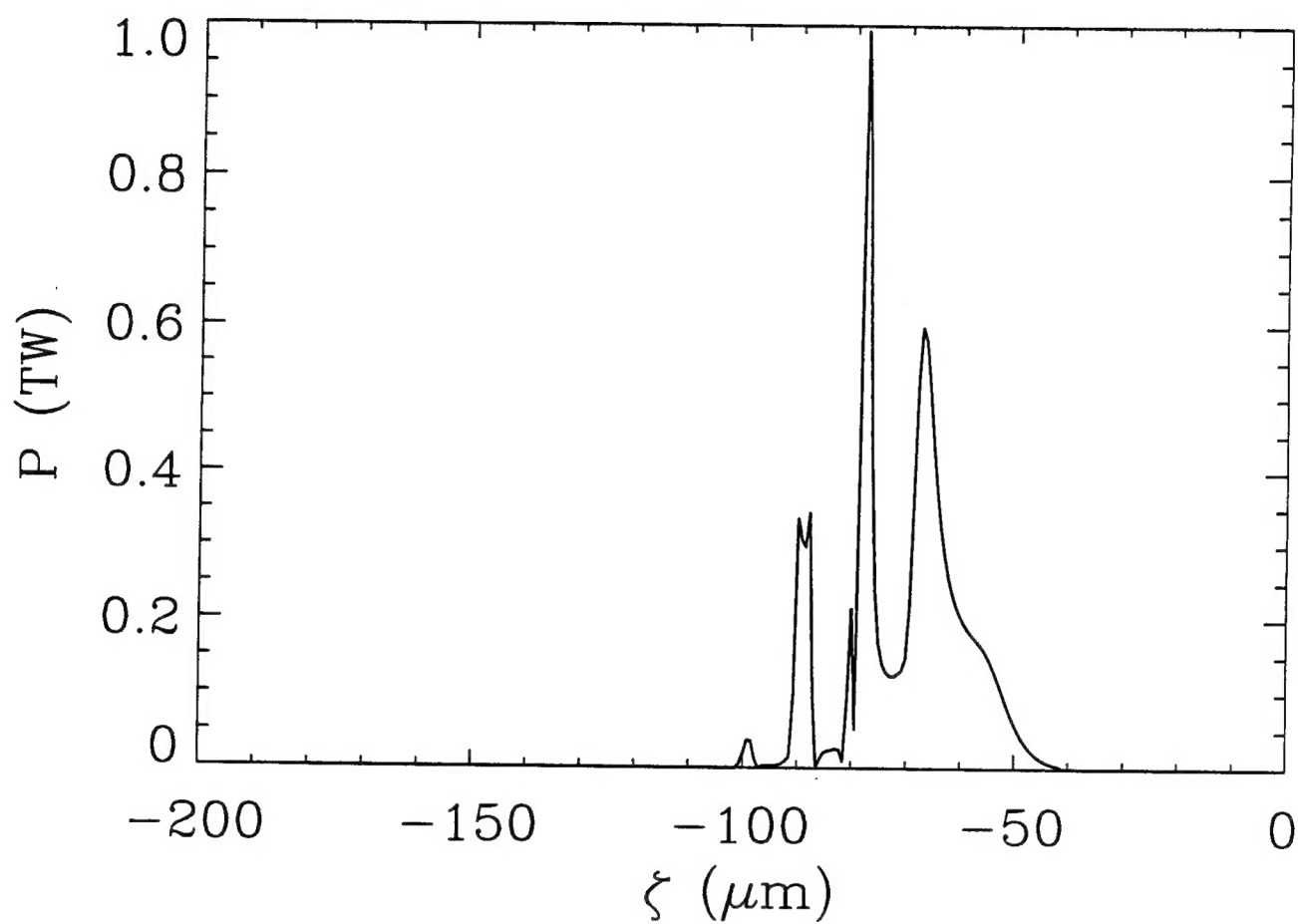
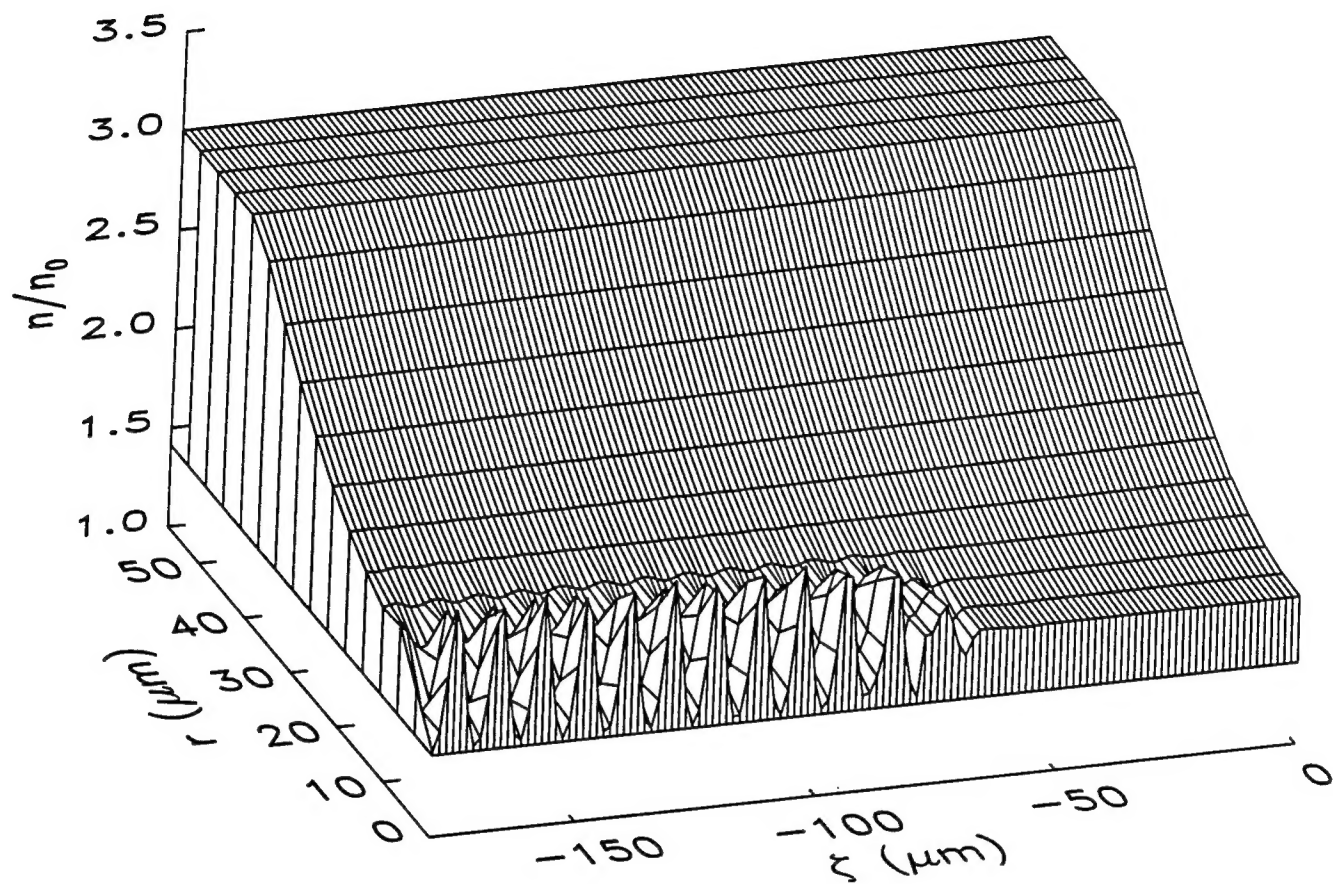Fig. 2 — Laser power P versus ζ at $c\tau = 0.75$ cm

17

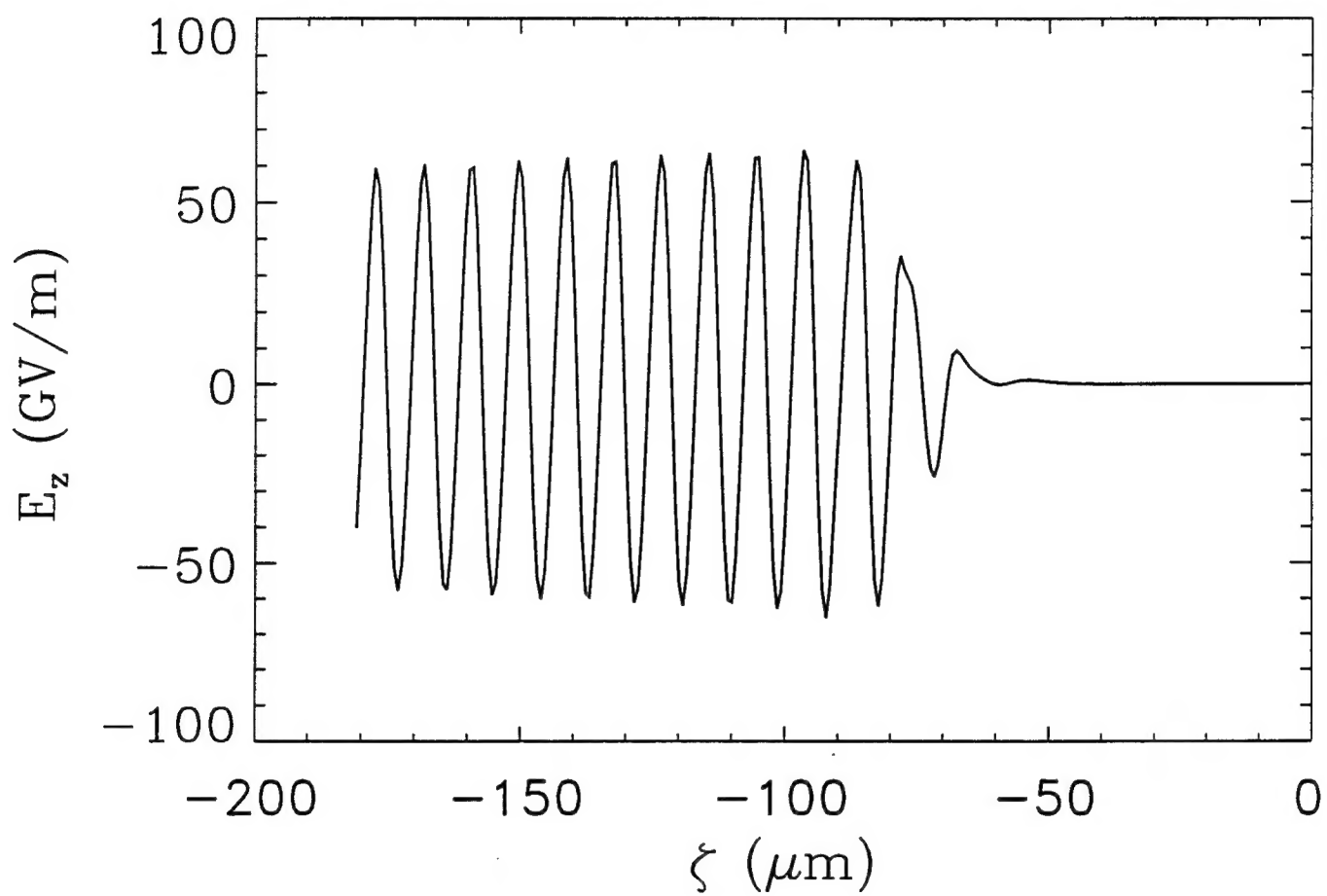Fig. 3 — Plasma electron density n/n_0 at $c\tau = 0.75$ cm

18

Fig. 4 — Electric wake field E_z versus ζ at $c\tau = 0.75$ cm